The Implication of the Connected Net Topology on the Morphology of β-Monoacid Triacylglycerol Crystals

F. F. A. Hollander,[†] S. X. M. Boerrigter,[†] J. van de Streek,[†] R. F. P. Grimbergen,[‡] H. Meekes,*[,†] and P. Bennema[†]

RIM Laboratory of Solid State Chemistry, Faculty of Science University of Nijmegen, Toernooiveld 1, 6525 ED Nijmegen, The Netherlands

Received: May 19, 1999

The crystal morphology of β *n.n.n* TAGs, still the only triacylglycerol series of which the crystallographic structures have been elucidated, is predicted using a revised version of the Hartman−Perdok theory. In an earlier publication by Bennema et al.[1] the morphology was predicted on the basis of attachment energy. The platelike shape of the crystals was predicted well, but the indices for the top faces failed. Second, the experimentally observed crystals are much more elongated. In the present approach, the morphology is not only predicted using the attachment energy but also use is made of roughening temperatures. For faces that grow below the roughening temperature at low supersaturation, the rate-limiting step is the formation of steps on the surface. Therefore, under these growth conditions, the roughening temperatures of the faces determine the morphology rather than the attachment of new growth units to the surfaces. The roughening temperature of a flat face {*hkl*} can be estimated by the Ising temperatures, which are calculated from substitute nets constructed from all possible step energies found from the connected nets. In some cases, depending on the topology of the connected net, exceptionally low Ising temperatures can be found. In these cases, it is shown that the roughening temperature is not directly determined by the slice energy. If this concept is used for the prediction of the morphology of TAG crystals, a good agreement with the experimentally observed faces is obtained. Moreover, the dependence of the morphology for the various TAGs on the chain length *n* is explained. Using this concept, however, the presence of the {31*l*} faces on the morphology cannot be explained. It is shown that this face is probably an F-face that is stabilized by solvent molecules.

Introduction

In a previous publication, the observed morphology of crystals of the β-2 polymorphic phase of monoacid triacylglycerol (TAG) crystals was explained on the basis of the crystallographic morphological theory of Hartman−Perdok (HP) and extensions to that theory taking into account the concept of surface roughening.[1] All TAGs, or fat molecules, are esterifications of three different fatty acids (R_1, R_2 and R_3) with glycerol. Therefore, we can abbreviate the nomenclature of the TAGs, according to de Jong[2] indicating merely the fatty acids used, i.e., $R_1.R_2.R_3$. For example, tripalmitate, which is an esterification of palmitic acid and glycerol, is denoted as 16.16.16. The TAGs used in this study are characterized by three identical, even numbered saturated alkane chains, denoted as *n.n.n*, and are the only TAGs of which the crystallographic structures have been elucidated.[3−6] For this series, all diffraction data show that the structures are homologous as was suggested by de Jong[7] and shown by van Langevelde et al.[6]

In the extensions to the HP theory, the concept of connected net plays an essential role.[8] One of the drawbacks of using connected nets is the frequently encountered large number of connected nets found for a single orientation (*hkl*) of crystals having more than one growth unit in the primitive cell. The ad hoc assumption used in such cases was that the strongest connected net of an orientation (*hkl*), that is the connected net with the lowest attachment energy, determined the morphological importance of that orientation. This was also the approach used by Bennema et al.[1] leading to a morphology that was only partly capable of describing the experimental data. Although the platelike morphology was predicted, the indices for the top faces failed.

The role of connected nets in the prediction of the equilibrium and growth morphology of crystals was reconsidered and given a physical foundation in a recent series of papers.[9−11] In these papers it was shown that the presence of multiple connected nets for an orientation (*hkl*) of the crystal can have an unexpectedly large influence on the equilibrium but especially the growth morphology of crystals. In particular the presence of more than one connected net for a single orientation (*hkl*) that are symmetry related by one of the space group symmetry elements of the crystal can lead to what was called symmetry roughening.[10] Symmetry roughening results, owing to an effective zero step free energy for steps on the surface, to a roughening temperature of zero Kelvin for the orientation (*hkl*) leading to rounded off or grown out facets. Also, pairs of connected nets of one orientation that are not symmetry related may lead to a very low effective step free energy resulting in a very low barrier for thermal or kinetic roughening. This phenomenon was called pseudosymmetry roughening. Corresponding orientations tend to have relatively large growth rates already at moderate supersaturations. Therefore, the growth rate as a function of supersaturation (driving force) can deviate

* Corresponding author. E-mail: hugom@sci.kun.nl.
[†] University of Nijmegen.
[‡] Present address: DSM research, P.O. Box 18, 6160 MD Geleen, The Netherlands.

10.1021/jp991634z CCC: $18.00
Published on Web 09/11/1999

significantly from that of an orientation which does not show symmetry or pseudosymmetry roughening. Such differences in growth rate versus supersaturation curves for different orientations can thus give rise to and at the same time explain growth morphologies that change with the driving force.[11]

TAG crystals also show a large number of connected nets for the orientations that are present on the relatively fast growing top faces of these crystals. The essential item of the HP theory is that all connected nets are made up of combinations of at least two periodic bond chains (PBCs). However, some connected nets contain more than two PBCs. These connected nets can give rise to a lowering in the Ising temperature, and therefore the roughening temperature, as will be explained in this paper. Moreover, it will be shown that, even in the case where there is merely a single connected net for an orientation {*hkl*}, a specific topology of the net can already lead to low effective step energies. In particular, it will be shown that the topology of the connected nets can explain the elongated morphology of TAG crystals. Using the effective step energies as derived from the topology and molecular interactions of the connected nets, the morphology of the TAG crystals is explained very well, even for varying chain length *n*.

This paper is organized as follows. First, some experimental results of the morphology of various TAG crystals within this homologous series are presented. Then the morphology is calculated using the revised Hartman−Perdok theory, taking into account the topology of the connected nets. In the last section, a comparison is made between this predicted morphology and the observed one.

2. Experimental Results

The experiments were carried out on TAGs with a purity of 99% (Sigma). All β_2-TAG crystals were grown using the same setup as described by Vogels et al.[12] An important difference between this setup and the one used by Skoda et al.[13] is that they used a dilatometer. This dilatometer keeps the supersaturation fixed, while in the setup used in our experiments the supersaturation decreased during growth. In Figure 1 three typical in situ crystals, grown under various conditions, are presented. For these in situ TAG crystals, only the *h* and *k* index could be determined easily. The *l*-index could only be determined ex situ. Many different crystallographic settings are used in the literature for the *n.n.n* TAGs, some even left-handed, which often leads to confusion. Luckily, all settings used can be simply transformed into one setting that represents all TAGs within this homologous series.[6] We use a setting based on the one left-handed setting presented by de Jong[7] and used by Bennema et al.[1], which makes the longest crystallographic axis the *c*-axis. The following transformation matrix converts their coordinate system $\boldsymbol{a}'$, $\boldsymbol{b}'$, $\boldsymbol{c}'$ into our $\boldsymbol{a}$, $\boldsymbol{b}$, $\boldsymbol{c}$:

$$\boldsymbol{a} = \boldsymbol{a}', \boldsymbol{b} = -\boldsymbol{b}', \boldsymbol{c} = \boldsymbol{c}' - \boldsymbol{b}'$$

The experimentally observed aspect ratio shows a weak dependence on the chain length and the supersaturation. On the average this aspect ratio for the length:width:height of the grown plates is about 50:5:1 for the crystals grown at low supersaturation. The crystals grown at high supersaturation became thinner and more platelike: the aspect ratio was about 100:50:1. On the average, the larger the chain length the more elongated the crystals was. This experimentally observed aspect ratio was, because of the growth conditions, difficult to compare with the calculated aspect ratio. As can be seen from Figure 1c, all TAG crystals grow mainly spherulitically, which will probably result that the local supersaturation at the top faces is higher than at the side and basal faces. Therefore, the experimentally observed platelike morphology can even be more exaggerated.

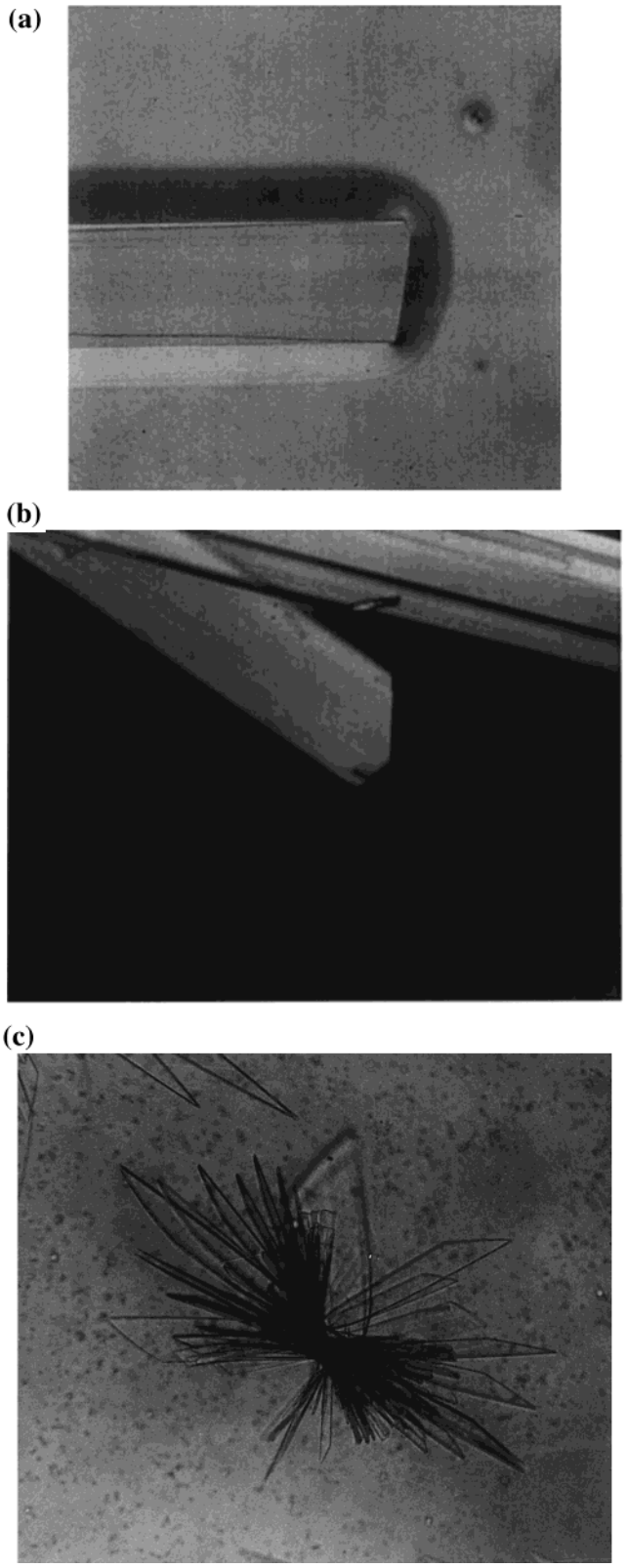

Figure 1. Typical top faces of TAG crystals grown under various circumstances. (a) A rare {11*l*} top face of 10.10.10. The *l* index is not determined. (b) A typical 16.16.16 crystal grown from an dodecane solution at a low supersaturation with a {21*l*} and a {01*l*} top face. (c) A 16.16.16 spherulite grown from a trioleate solution at high supersaturation with thin platelike crystals with rounded {*h*1*l*} faces, where *h* is either $\bar{2}$, $\bar{1}$, or 4.

TABLE 1: Top Facets Observed for the Different TAGs Using the Optical Microscope; Present Results,[P] Those of Albon and Parker[A,15] and Skoda et al.[S,13,14,a]

	10.10.10	14.14.14	16.16.16	18.18.18	22.22.22
{01*l*}	L++[P]	L++[P]	L++[P,A,S]	L++[P,S]	L+[P]
{11*l*}	L+[P]				
{21*l*}	L++H++[P]	L++[P]	L+++[P,S]	L++[P,S]	L+[P]
{3̄1*l*}		L+[P]	L+[P,S]	L+[P,S]	
{1̄1*l*}			H+[P]		
{2̄1*l*}					
{41*l*}					

[a] The rate of occurrence is given with the number of +'s. Because of scattering it is hard to decide whether the sharp needles at high supersaturation (Figure 1c) are {41*l*}, {2̄1*l*}, or {1̄1*l*} faces. The growth conditions are indicated by (L)ow or (H)igh supersaturation. All crystals are grown from a trioleate or alkane solution, except for 10.10.10 which are grown from an acetone solution.

Because TAG crystals, especially the longer TAGs (18.18.18 and 22.22.22), grown from a trioleate solution show a large shut-off effect, the crystals for studying the morphology ex situ were grown from *n*-alkane solutions. The following crystals were grown: 14.14.14 from decane, 16.16.16 and 22.22.22 from a dodecane, and 18.18.18 from a tetradecane solution. The 10.10.10 TAGs crystals were grown from acetone by evaporation. After one to three weeks the crystals, which grew spherulitically, were removed from the solution. On removal, the spherulites broke up in lots of single crystals showing large {001} basal faces, flat side faces, mostly {100}, sometimes {101}, and various faceted top faces. The facets were indexed by optical microscopy or using an optical goniometer. Using the optical microscope only resolves the *h* and *k* indices of the top faces, because of the platelike morphology of the crystals. Remember that for these homologous series of TAGs the *a*- and *b*-axes are approximately constant, which results in almost identical angles for specific *h* and *k* indices, independent of the TAG. When the optical goniometer is used instead, the *l*-index can also be resolved. However, it is quite hard to resolve this *l* index, and the results are not totally reliable as they show a lot of scattering between various crystals, especially for the {01*l*} faces. These difficulties are due to poor reflections, easily bent crystals, and shut-off effects in combination with the relatively long *c*-axes. The calculated deviations in the angles for the various alternatives of the *l* index are only a few degrees and were often within the margin of error. For crystals grown at high supersaturation, sharp platelets were found, as can be seen in Figure 1c. Using the optical microscope to determine the *h*-indices, the data show a lot of scattering partially because these faces are somewhat rounded off. Therefore the faces are hard to identify, especially because the angles with respect to the basal face for the {2̄1*l*}, {1̄1*l*}, and {41*l*} faces are 33, 42, and 40 degrees, respectively. The average experimental value found was 37 ± 8 degrees.

The results of these morphology measurements can be found in Tables 1 and 2, including the result of previously published work.[14,15]

3. Connected Net Analysis

For the determination of the connected nets of these TAG crystals, a procedure similar to the one of Bennema et al.[1] is used, based on the classical Hartman−Perdok theory.[8,9,16] This analysis can be divided into four steps, the calculation of the intermolecular interactions, the building of the crystal graph, the determination and analysis of the connected nets and the final morphology construction.

TABLE 2: Facets Observed for 16.16.16 and 18.18.18 Using the Goniometer; Present Results[P] and Those of Skoda et al.[S,13,14,a]

	16.16.16	18.18.18
{01*l*}	{01$\bar{2}$}[S] {01$\bar{1}$}[P]	{01$\bar{2}$}[S]
{11*l*}		
{21*l*}	{211}[P,S]	{211}[S]
{31*l*}	{311}[P,S]	{311}[S]

[a] For both analyses, the {001} face is used as a reference. All measured crystals were grown at low supersaturation. For the other observed top faces mentioned in Table 1, the crystals are too thin to determine the *l*-index.

3.1. Calculation of the Intermolecular Interactions. The intermolecular interactions needed for the connected net analysis were recalculated using the consistent valence force field[17] and compared to those calculated by Bennema et al.[1] This force field was chosen because it provides atomic charges for molecules with these large numbers of atoms in a computationally inexpensive way. The experimental coordinates are available only for 10.10.10, 12.12.12, and 16.16.16, and to obtain a consistent series (especially for the position of the hydrogen atoms), the missing structures were assembled by elongating the alkane chains and the *c*-axes. The *x*, *y*, and *z* coordinates of the glycerol backbone atoms of 10.10.10, 12.12.12, and 16.16.16 were averaged. The 12.12.12 structure by Larsson[5] was omitted because of its large *R* value ($R = 0.20$). For all structures, the crystal energy was minimized using molecular mechanics. However, during energy minimization the glycerol backbone deformed as a result of intramolecular stress. Since it is only the *inter*molecular interactions we are interested in, it was decided to fix the carbon and oxygen atoms of the glycerol backbone during energy minimization.

For each TAG structure, a list of intermolecular interaction energies was calculated by subtracting the intramolecular energies from its total energy. The interaction energies for the various TAGs are given in Table 3. Note that although the space group is P1̄, the molecular interactions do not show this symmetry, because the center of symmetry is in the middle of the interactions between the two molecules in the unit cell. The five molecular interactions in the lower part of Table 3 were not considered in the final analysis, because their influence is negligible.

From this list of intermolecular interactions, a selection of strong interaction energies, forming the crystal graph, is taken to predict the morphology. The crystal graph consists of the centers of mass of the TAG molecules and a set of interactions. For the present study, two different crystal graphs were used. The smallest data set included only the seven strongest interaction energies, while for the intermediate data set the same cutoff energy as that of Bennema et al. was used.[1] This cutoff energy of 1.0 kcal/mol results in 13 different molecular interactions. The t_1 and q_4 interactions were additional to the set of Bennema et al. The crystal graphs, including the corresponding crystallographic unit cell, for the two different data sets are depicted in Figure 2.

The two crystal graphs were used as input for the FACELIFT program,[18] which is an automation of the connected net analysis and is included in the Cerius[2] package[19] as the Hartman−Perdok module. This module searches for periodic bond chains (PBCs) and combines these into connected nets.[9] These connected nets were used for further analysis. The prediction will be worked out in detail for the first data set, and thereafter the results for the intermediate data set will be discussed.

TABLE 3: Different Interaction Energies in Kcal/Mol for the Various TAGs[a]

interaction	$CM_i \cdot M_j$-[$u\bar{v}w$]	10.10.10	12.12.12	14.14.14	16.16.16	18.18.18	20.20.20	22.22.22
p	1.1-[0$\bar{1}$0]	−21.7	−25.4	−29.0	−32.6	−36.3	−39.8	−43.4
r_2	1.2-[$\bar{1}$00]	−19.8	−22.9	−26.0	−29.1	−32.2	−35.3	−38.5
q_2	1.2-[0$\bar{1}$0]	−20.7	−23.3	−25.9	−28.6	−31.3	−34.0	−36.8
r_1	1.2-[$\bar{1}$10]	−16.1	−18.8	−21.5	−24.3	−27.1	−29.9	−32.8
q_1	1.2-[000]	−14.4	−17.6	−20.8	−24.0	−27.1	−30.3	−33.5
s_2	1.2-[00$\bar{1}$]	−2.9	−2.9	−2.9	−2.8	−2.8	−2.8	−2.8
s_1	1.2-[0$\bar{1}\bar{1}$]	−2.5	−2.5	−2.5	−2.5	−2.5	−2.5	−2.6
q_4	1.1-[$\bar{1}$00]	−1.1	−1.3	−1.6	−1.8	−2.0	−2.3	−2.5
r_3	1.2-[$\bar{1}\bar{1}$0]	−1.2	−1.4	−1.6	−1.7	−1.9	−2.1	−2.3
q_3	1.2-[0$\bar{2}$0]	−1.1	−1.3	−1.5	−1.7	−1.8	−2	−2.2
r_0	1.2-[$\bar{1}$20]	−1.1	−1.2	−1.4	−1.6	−1.7	−1.9	−2.1
q_0	1.2-[010]	−0.6	−0.8	−1.0	−1.2	−1.3	−1.5	−1.7
t_1	1.2-[$\bar{1}\bar{1}$1]	−1.1	−1.0	−1.0	−1.0	−1.1	−1.1	−1.1
q_5	1.1-[1$\bar{1}$0]	−0.4	−0.5	−0.6	−0.7	−0.8	−0.9	−0.9
q_6	1.1-[110]	−0.4	−0.5	−0.6	−0.6	−0.8	−0.9	−0.9
s_3	1.1-[10$\bar{1}$]	−0.7	−0.7	−0.7	−0.7	−0.7	−0.7	−0.7
s_4	1.1-[00$\bar{1}$]	−0.6	−0.6	−0.6	−0.6	−0.6	−0.6	−0.6
t_2	1.2-[$\bar{1}$11]	−0.6	−0.6	−0.6	−0.6	−0.6	−0.6	−0.6

[a] In the second column, the directions of the PBCs are listed, where, $CM_i \cdot M_j$-[$u\bar{v}w$] denotes the interaction energy between molecule i and another molecule j of a second unit cell translated over a lattice vector [$u\bar{v}w$]. For the strong p-interaction, the energy is given as the sum of 1.1.-[0$\bar{1}$0] and 1.1-[0$\bar{2}$0]. The labels of the different interactions are identical to those used by Bennema et al.[1]

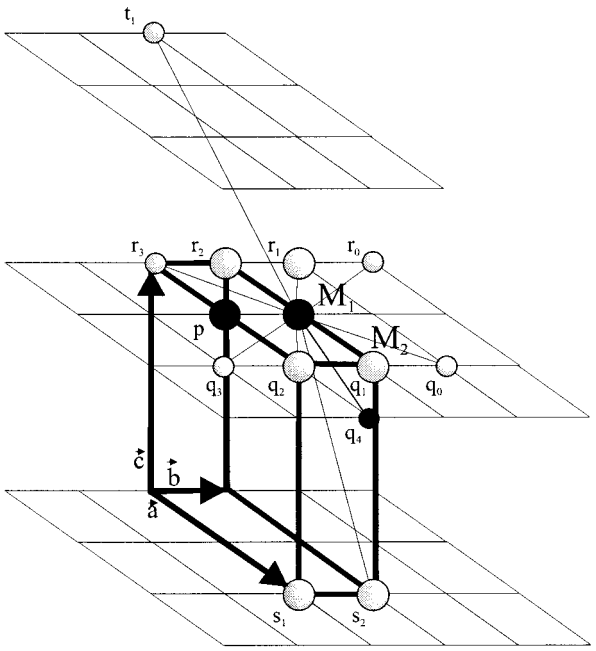

Figure 2. Two crystal graphs considered, including the unit cell, which contains two TAG molecules labeled M_1 and M_2. All translationally symmetric equivalents of M_1 are colored black, while the white spheres are equivalent to M_2. The molecular interactions of interest are the interactions between the large sphere M_1 and the other spheres given. The label for the molecular interaction is indicated at the end molecule. The seven large spheres, excluding M_1, make up the small data set, while the set of all spheres also includes the additional molecular interactions for the second, intermediate data set.

3.2. Connected Net Determination and Analysis. Using the first data set, the FACELIFT program finds 13 different PBCs. After combining these PBCs, besides the {001} basal face and the {100} and {101} side faces, eight different possibilities for the top faces are found. Note that for the top faces, the h index of the face is determined by the PBC that is formed by a combination of one q interaction and one r interaction. The additional s interaction needed to complete the connected net determined the l index. The connected nets are listed in Table 4.

In the classical Hartman−Perdok theory, taking surface roughening into account, the roughening temperatures and attachment energies of the connected nets are calculated to construct the morphology using a Wulff−Herring construction as was done by Bennema et al.[1]

TABLE 4: Connected Nets Found by FACELIFT with Their Attachment Energies[a]

face	{hkl}	$E_{attachment}$ (kcal/mol)	# connected nets
B	{001}	−5.2	1
S_1	{101}	−52.5	1
S_1	{100}	−52.6	1
T_1	{111}	−113.5	1
T_2	{110}	−113.7	2
T_3	{211}	−117.5	1
T_4	{210}	−117.7	1
T_5	{010}	−118.1	1
T_6	{01$\bar{1}$}	−118.3	1
T_7	{11$\bar{1}$}	−122.3	1

[a] The faces are denoted according to their type ((T)op, (S)ide, or (B)asal).

For the roughening temperatures, usually the Ising temperatures of the connected nets are used as a good approximation.[20] In that approach, a rectangular equivalent of the connected net is constructed to calculate the Ising temperature.

3.3. Roughening Temperatures. According to the criterion of van Beijeren and Nolden[21] a face will only grow flat if the following condition is fulfilled. Every flat face (i.e., a crystal face below the roughening temperature) has the property that the sum of the step free energies, for a step up and a step down, is larger than zero for every direction [$u\bar{v}w$] parallel to the face (hkl). For the usual calculation of the Ising temperature, as an estimate for the roughening temperature,[20] a distinction between attachment and slice energy is made. The interactions that make up the slice energy then determine the Ising temperature. This approach is however not always correct. An example of a nonstraightforward connected net that is characteristic for the TAG top faces is depicted in Figure 3. In this figure, a bricklike pattern is drawn. Grimbergen et al.[9] have shown that for a similar cubelike pattern, which includes one extra molecular interaction, such faces show pseudosymmetry roughening. The pattern of Figure 3 is a two-dimensional projection of a connected net that is made up of a and b interactions together with interactions perpendicular to the drawing. The connected nets are mutually connected by the interactions c.

From a close examination of the topology of the connected nets, analogous to Grimbergen et al.,[9] the effective step energy

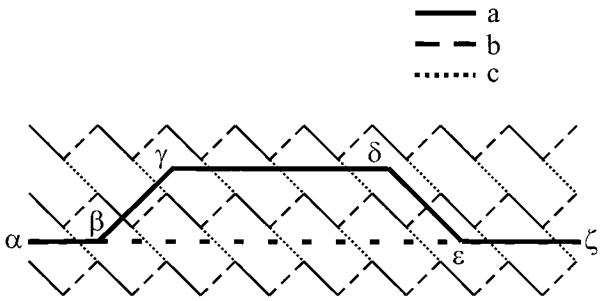

Figure 3. Brick-layered structure made up of molecular interactions *a* and *b* and a third one along the projection. The resulting connected nets are interconnected by a third molecular interaction *c*. The effective energy of a step can be calculated as the difference in broken bond energy of the stepped interface $\alpha\beta\gamma\delta\epsilon\zeta$ and the flat interface $\alpha\beta\epsilon\zeta$ as indicated. For the down step, this results in a step energy that is determined by the difference in interaction energies *b* and *c*, while for the up step only the interaction energy *a* is involved.

can be calculated as the difference in broken bond energy of the stepped interface $\alpha\beta\gamma\delta\epsilon\zeta$ and the flat interface $\alpha\beta\epsilon\zeta$ indicated. This energy is then given by $(\Phi_a + \Phi_b - \Phi_c)$, where Φ_i is the energy of interaction *i*. In the usual approach, the attachment energy is made up by the *c* interaction and the slice energy by the interactions that make up the connected net. However, this classification is not appropriate for calculating the Ising temperatures. If the energy difference between the *b* and *c* interactions is small, then the down-step $\gamma\delta\epsilon\zeta$ has a low energy, namely the energy difference $\Phi_b - \Phi_c$. Conversely, the up-step $\alpha\beta\gamma\delta$ has an energy Φ_a. In the classical approach[8] the step energies would be identical to the slice energy, thus Φ_b and Φ_a, respectively.

To estimate the Ising temperature of such a connected net, however, a substitute connected net can be constructed using the effective step energies for all directions [*uvw*].[11] These effective step energies can be calculated using the recipe of broken bond energies, as mentioned above. Every step direction has a step up and a step down which differ in energy. Therefore, a substitute net that explicitly includes both the step up and the step down would have a too low Ising temperature, as such a net allows for two-dimensional nuclei made up of only the steps with the smallest energy. The topology of the connected net shown in Figure 3, on the other hand, ensures that a two-dimensional nucleus always consists of both a step up and a step down. Therefore, the probability of creating such nuclei depends on the sum of the energies of a step up and a step down, and the Ising temperature is the same as that of a comparable connected net as in Figure 3 with both the step up and step down energies equal to the average of the step energies of Figure 3. The substitute net can now be created from all positive averaged step energies found. If no positive step energy is found within all directions [*uvw*], the face {*hkl*} grows rough according to the criterion of van Beijeren and Nolden. In the case that positive step energies are found in at least two different directions, which can only be the case for connected nets, the face grows flat. For these faces, the Ising temperatures of the substitute nets are used as an estimate for the roughening temperatures. Using the concept of difference interactions, the Ising temperature can decrease dramatically, especially when, the total step energy of both the up step and down step is small. However, because we are averaging the total step energy, this also holds for steps that have a negative energy of the step up (or step down) but a larger positive energy for the step down (or step up) or vice versa.

Remember that the molecular interactions were calculated for growth from the vapor, while all TAG crystals are grown

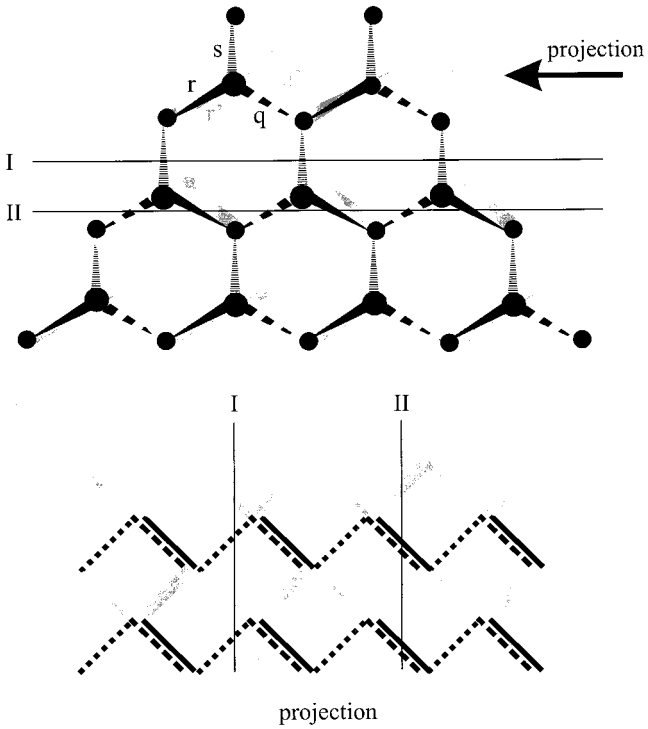

Figure 4. (a) Top view of the honeycomblike structure of the {110} top face resulting from the small data set; the energetically most favorable steps are indicated by the roman numbers I−III. (b) Projection of the honeycomb-like structure, resulting in a Grimbergen et al.[7]-like structure for the {110} top face and a brick-layered structure, cf. Figure 3, for the other top faces.

from solution. Therefore, the absolute values of the Ising temperatures cannot be related directly to the roughening temperatures. It is assumed that $T_I = \alpha T_R$, where T_I is the Ising temperature of the substitute net and T_R is the roughening temperature of the face {*hkl*}. The proportionality factor α can be determined if one roughening temperature is known, i.e., experimentally observed. So far, no roughening temperatures for TAGs are known. Nevertheless, the Ising temperatures result in good indications for the step energies that determine the growth, especially at low supersaturation.[9]

3.4. The Ising Temperatures for the Small Data Set of the TAGs. For the TAG crystals, the concept of effective Ising temperatures given above is of crucial importance to the roughening temperatures of the top faces. The connected nets of the side faces {100} and {101} and the basal faces {001} are trivial in the sense that the topology does not give rise to small difference interactions. Therefore, the Ising temperatures can be calculated straightforwardly.[20] For, 16.16.16, the calculated Ising temperatures are 5470, 5480, and 15900 K for the {100}, {101}, and {001} faces, respectively, using the small data set. Although only the {100} side faces are reported by Skoda et al.[13,14] one cannot easily distinguish between the {100} and {101} side faces using Ising temperatures, calculated from the small data set only. We have occasionally observed the {101} side face.

For the small data set the connected nets of the top faces are all formed by a honeycomb-like structure of one *r*, one *s*, and one *q* molecular interaction from Table 3, in a tripod configuration. The {110} face, which contains two connected nets, consists of a complete tripod−antitripod configuration, i.e., all directions *r*, *s*, and *q* also have an alternative *r*′, *s*′, and *q*′, as is depicted in Figure 4. The two different tripods are drawn in different gray levels. The other six possible top faces always

have one interaction of these six interactions missing, resulting in only one single connected net. Despite, the presence of only one single connected net, three different PBCs are situated within one slice, with thickness d_{hkl}.

To estimate the roughening temperatures of these top faces, the steps with the lowest energy have to be determined. In the same Figure 4, a projection is made along the horizontal direction of the top view, resulting in a rooflike pattern for the {110} face, analogous to Grimbergen et al.[9] For this honeycomb-like structure, the candidates for the low-energy step directions are given by a Roman numeral in Figure 4. Note that for this projection, step direction II is given by the interactions, r/r' and q/q', projected onto each other. For the other projections that are rotated over 60 and 120 degrees, resulting in similar figures, all possible step directions are given by a combination of interactions projected onto each other. Remember that two step directions are always needed to create an island with a step up and step down, but the corresponding step energy may differ whether the step direction serves as a step up or a step down. Using these projections, the averaged step energies can be estimated by calculating the broken bond energies, in the same way as was mentioned above.

From all step energies found, different substitute nets can be created which represent the flat face {*hkl*} with a specific type of two-dimensional island. For all of these substitute nets, the Ising temperature was calculated using the method of Rijpkema et al.[20] The lowest Ising temperature calculated from all substitute nets found was used as an estimate for the roughening temperature for this face {*hkl*}. It can be seen that for this {110} face, containing two connected nets, difference interactions always apply for at least one of the possible steps, i.e., step up or step down. Especially, in this case for the {110} face, it can be seen that the difference interactions are small, because both interactions within the interaction pairs r_1/r_2, s_2/s_1, and q_1/q_2 are of the same order. Therefore, the Ising temperature calculated for this face is low, compared to an Ising temperature calculated from the classical approach that uses the slice energy of the connected net.

For the remaining top faces with only one connected net, the same method as described for the {110} face can be used to calculate the Ising temperature. However, because one interaction is missing, the effect on the roughening temperature is not as dramatic as for the {110} face. The results of the calculated Ising temperatures for the various TAGs are given in Figure 5. From this figure, it can be seen that the {11*l*} faces are approximately independent of or even weakly decreasing with the chain length *n*. For the other top faces, the dependence is roughly increasing linearly.

The resulting Ising temperatures for the {21*l*} and {01*l*} faces are the highest, especially for the longer TAGs, which is in agreement with the experiments. For 10.10.10, the Ising temperatures of the {111} faces are comparable to those of the {210} faces. This explains that sometimes {11*l*} faces are observed for these shorter TAGs.

Although the small data set describes the experimental morphology in detail, the {311} faces, which are observed experimentally according to Table 2, are not present. Second, the possible faces that are present at high supersaturation for 16.16.16, i.e., $\{\bar{2}1l\}$, $\{\bar{1}1l\}$, and/or {41*l*}, are not connected. Therefore, the set of molecular interactions has to be extended to the intermediate set.

3.5. The Effect of Adding More Molecular Interactions. If the number of molecular interactions is increased to the intermediate data set, the number of PBCs and connected nets increases to 43 and 59, respectively, resulting in 35 different F-faces. This implies that the analysis becomes more complicated, because all possible steps have to be determined for all connected nets found. Especially, the topology of the connected nets of the side and basal faces becomes involved, because of the extra molecular interactions that are present in the slice {*hkl*}. However, still no energetically favorable steps can be made, which could result in a dramatic decrease of the Ising temperature compared to the small data set. Therefore, the Ising temperatures calculated from the small data can be regarded as good estimates for the Ising temperature of the intermediate data set. Besides the Ising temperatures, the attachment energies are also influenced, because more interactions are taken into account. Calculated Ising temperatures and attachment energies for the most important faces are given in Figures 5, 6, and 7, respectively, both as functions of the chain length *n*.

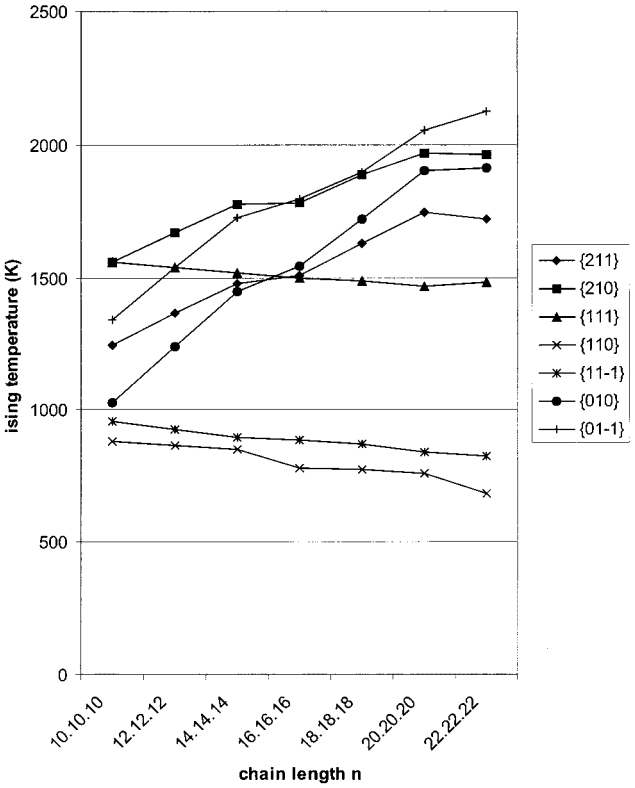

Figure 5. Ising temperatures T_C in K for the various TAGs for the small data set. The various faces are ranked in the legend according to the Ising temperature of 22.22.22.

The general honeycomb-like structure as given in Figure 4 for the various top faces hardly changes. This minor effect is the result of the fact that the additional interactions are an order of a magnitude smaller than the seven strongest interactions. This implies that the Ising temperatures for the faces already present in the small data set hardly change. The results for the 22 strongest faces of this set can be found in Figure 6. This set of faces is identical to that of Bennema et al.[1] Although the intermediate set results in more connected nets than the set used by Bennema et al., the rest of the F-faces found includes the weakest interaction t_1, which always results in low Ising temperatures and high attachment energies. Therefore, these faces are not considered further.

It can be seen that, on the average, the $\{21\underline{l}\}$ and $\{01\underline{l}\}$ faces still have the highest Ising temperatures. The $\{\bar{2}1\bar{1}\}$, $\{\bar{2}1\underline{2}\}$, and the {411} faces, which are now also connected have Ising temperatures comparable to these {01*l*} and {21*l*} faces. Besides high Ising temperatures, these new faces also have high

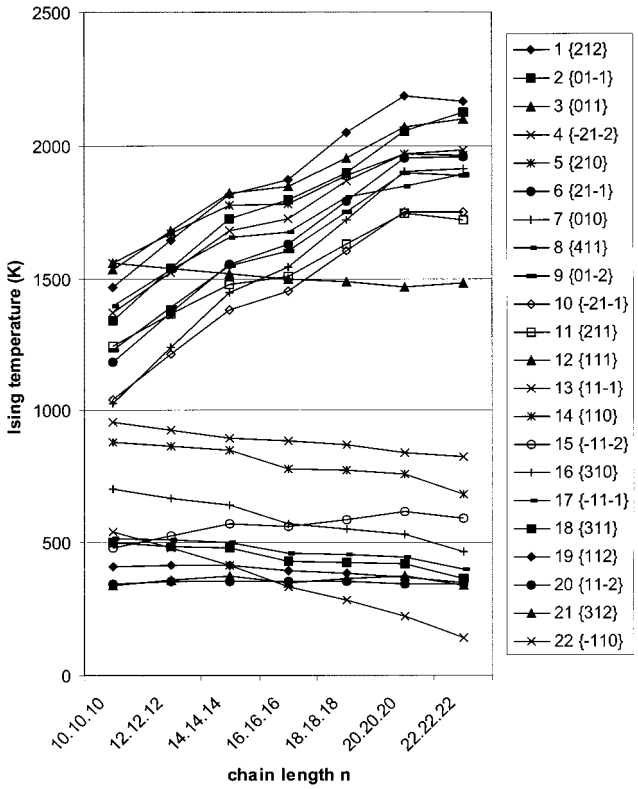

Figure 6. Ising temperatures T_C in K for the various TAGs for the intermediate data set. The various faces are ranked in the legend according to the Ising temperature of 22.22.22.

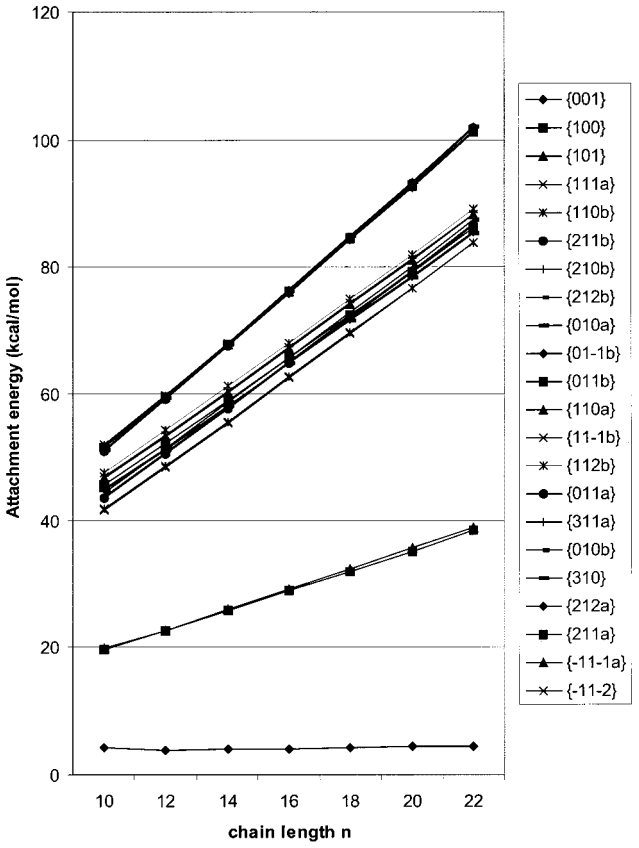

Figure 7. Selection of the 22 *n.n.n* TAG faces with the lowest values for the attachment energies of the intermediate data set. Note that the legend is ranked differently compared to Figures 5 and 6. For some doublet faces {*hkl*}, which are given an extra label *a* or *b*, different connected nets are possible.

attachment energies, which are even outside the range of the faces given in Figure 7. Therefore, the faces given are not likely to appear on the morphology, although these faces were possible candidates for the faces observed at high supersaturation for 16.16.16.

The other experimentally observed face that was missing is the {311} face. The Ising temperature of this face is lower than that of the {111} face, which is never observed for the longer TAGs, while the {311} face is observed for these longer TAGs. Therefore, predicting the morphology on the basis of the Ising temperature and/or attachment energy excludes this {311} and, in fact, all {31*l*} faces from being present on the morphology.

If we consider the *l*-index for 16.16.16 and 18.18.18 (cf. Table 2), it can be seen that, for the small data set, the $\{01\bar{1}\}$ and {210} have the highest Ising temperatures. Experimentally, the {211} and $\{01\bar{2}\}$ or $\{01\bar{1}\}$ were observed. This means that the *l*-index for only the {01*l*} face is in agreement with our measurements. However, the possible *l*-indices for the {21*l*} and {01*l*} faces all correspond to Ising temperatures which are high and lying close together and are therefore assumed to be possible candidates to appear on the morphology. Moreover, it is possible that more than one face, which differ only in *l*-index, are simultaneously present on the morphology.

Extending the set of molecular interactions with all interactions mentioned in Table 3, no new F-faces are found having Ising temperatures or attachment energies comparable to the faces already found. Therefore, the criterion used of 1 kcal/mol appears to be sufficient.

4. Summary and Discussion

The morphology is predicted well for low supersaturation, apart from the appearance of the {311} faces, using only the seven strongest molecular interactions using the revised interpretation of the HP theory. This indicates that considering roughening temperatures, besides attachment energy, as a predictive tool is essential. Note that no expression for the growth rate based on the estimated roughening temperatures is assumed for the morphological importance of the faces found, such as, for example, ($R_{hkl} \propto 1/T_i$). It is shown, however, that each flat face that appears on the morphology, which is not reconstructed or influenced by solvent molecules, must fulfill three conditions rather than two in the classical HP theory. These conditions are that each F-face found from the HP theory must have both a large roughening temperature and a low attachment energy. It is shown that these latter two conditions are not simply related by the slice energy.

Considering the top faces of the TAG crystals, it is assumed that for low supersaturation the growth mechanism is mainly dominated by two-dimensional nucleation or spiral growth. Although growth spirals have been observed on the {001} faces,[22] it is not likely they appear on the small top faces because they can easily grow out of the crystal. Hence, two-dimensional nucleation is more likely to be the main growth mechanism for the top faces of the TAGs considered. For this growth mechanism, the creation of steps is the rate-limiting step and, thus, the lower the roughening temperature, the lower the effective step energy and the higher the growth rate. Therefore, the roughening temperature is a good indication for the growth rate at low supersaturation. The roughening temperature can be estimated by calculating the Ising temperature from all possible step energies found for each particular face {*hkl*}. The step energies can be found by considering the connected net topology found from the HP theory and calculating the broken bond energy of a flat face with a stepped face. The lowest Ising

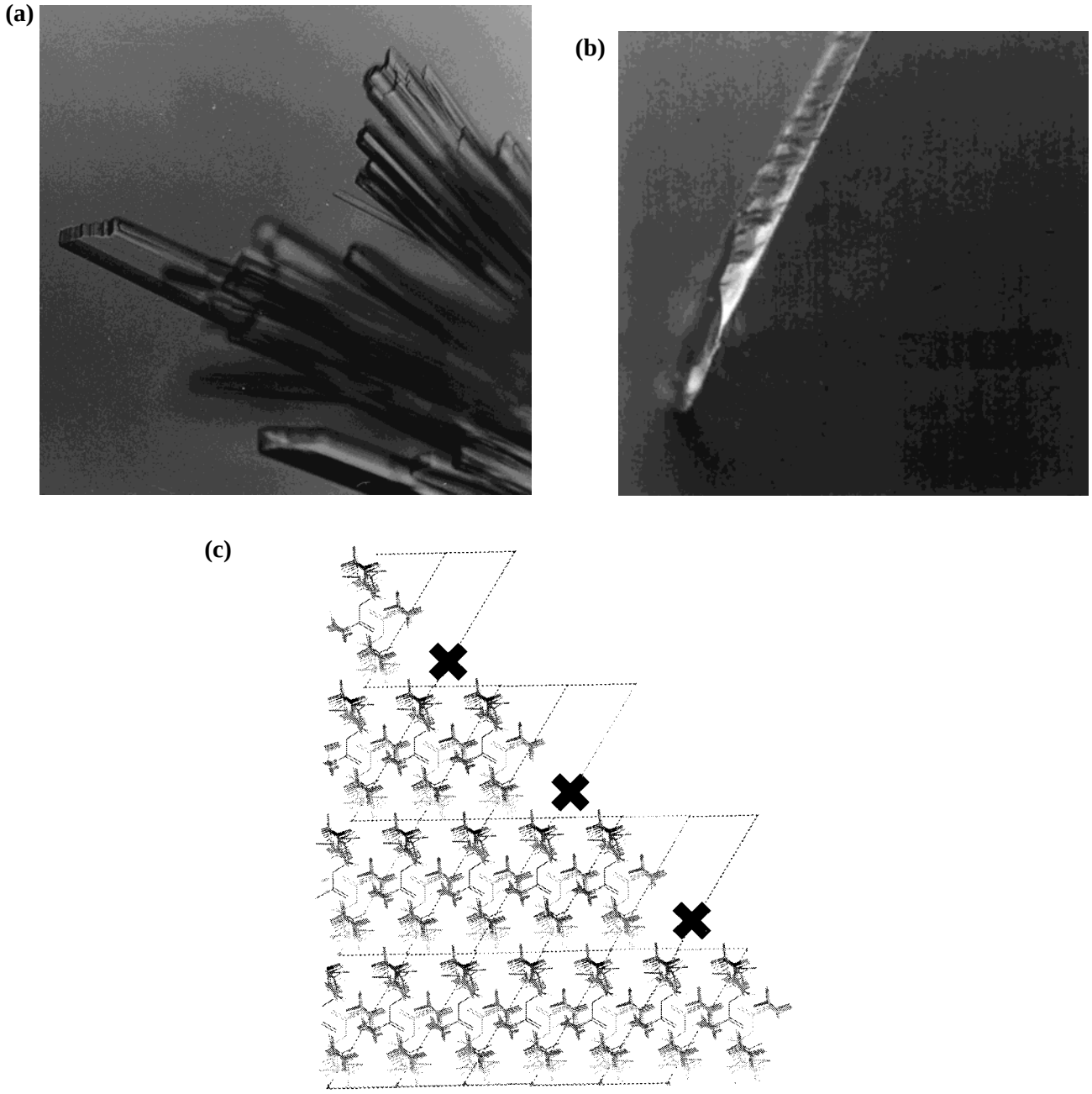

Figure 8. Closer examination of the {311} top face. (a) The breaking up of this face into {21*l*} and {010} faces for increasing supersaturation. (b) Optical micrograph of the surface of a {311} top face, already showing the microscopic breaking up for a crystal grown at small supersaturation. (c) Projection of one layer of the {310} faces along the *c*-axis. The *b*-axis is horizontal. The crosses indicate the hydrophobic positions for the solvent molecules (dodecane, trioleate).

temperature calculated is then used as the estimate for the roughening temperature. The faces with the highest Ising temperatures calculated are then the important faces on the morphology at low supersaturation.

It is shown that for *n.n.n* TAGs the morphology prediction results in mainly two different morphologies as a function of the chain length *n* when taking Ising temperatures into account. For the longer TAGs, the {01*l*} and {21*l*} faces are found to be the most important faces, while only for the shorter TAGs the {111} faces are also important, which agrees with the experimentally observed top faces. For the intermediate set, also the $\{\bar{2}1\bar{1}\}$, $\{\bar{2}1\bar{2}\}$, and {411} faces are connected and have comparable Ising temperatures to the {01*l*} and {21*l*} faces. However, these extra faces also have high attachment energies, which makes them unlikely to be present at the morphology. Remember that if the morphology was predicted using the attachment energy only, as was done by Bennema et al.,[1] the {11*l*} faces are the most important faces, independent of the chain length *n*. Although, for TAGs the determination of the *l*-index of the top faces is hard, it is shown that even this *l*-index can be predicted reasonably.

Nevertheless, the {311} face, which was found experimentally for low supersaturation, remained missing in a prediction based on Ising temperatures and/or attachment energy. As mentioned by Skoda et al.,[13] and can be seen in Figure 8a, this face roughens easily when the supersaturation is increased during growth and breaks up in {01*l*} and {21*l*} faces. This implies that the step energy is not as high as the calculations suggest. A closer examination of these faces shows that they are not as flat as other top faces observed on TAGs. A typical surface of

a {311} face is shown in Figure 8b. This face already shows the breaking up of the face on a much smaller scale. A possible explanation for the presence of this face is that it is blocked by solvent molecules, which results in a solvent-stabilized F-face. As can already be seen from Table 1, the 10.10.10 crystals, which were grown from an acetone solution, did not show this {311} face. An examination of this face using Cerius[2,19] showed that these faces contain kink positions that are very hydrophobic. These kink positions can easily be filled up by apolar solvent molecules, such as, for example, alkanes or trioleate, as is shown in Figure 8c. At higher supersaturations this blocking effect is expected to be overcome, resulting in {010} and {21*l*} faces.

The Ising temperatures of the basal, side and top faces for 16.16.16 have a mutual ratio of 9:3:1, which is comparable with the aspect ratio found from a prediction based on the attachment energy only. For a comparison with the experimental aspect ratio, however, the different relevant growth mechanisms for these faces have to be known. Moreover, as mentioned before, the aspect ratio is probably influenced by the spherulitical growth mechanism.

At higher supersaturation, the growth rate of the faces will not be determined by the formation of steps on the surface anymore, because of a decrease of the size of the critical nucleus. The growth morphology will then be mainly dominated by faces with low attachment energy. In the case of the shorter TAGs, this would imply that the {11*l*} faces should be the most prominent faces, followed by the {21*l*}, and maybe {01*l*} faces. For 10.10.10, the {21*l*} faces have been observed to be the most important top faces, which slowly disappear during the experiment, and {11*l*} top faces take over at the end of the experiment, i.e., for a small supersaturation. Therefore, it is only partly satisfactory for the case of 10.10.10. However, for 16.16.16 none of these faces was observed at all. Here, the possible faces observed were the $\{\bar{2}1l\}$, $\{\bar{1}1l\}$, and/or {41*l*} faces which all have a relatively high attachment energy. This is, however, converse to the argument that for increasing supersaturation the attachment energy becomes the most important parameter for the morphological importance of the faces. A possible explanation would be that the appearance of these faces is an effect of the solvent. As can be seen in Figure 1c, the faces observed are not nice straight faces. Second, it is known that fats crystallize in different polymorphs, under various conditions. For example, Kellens et al.[23] showed that four different β' polymorphs were found, besides the present β polymorph, when crystallizing 16.16.16 from the melt. Moreover, they showed that both polymorphs, β and β', can be simultaneously present in the crystallization process. However, if we assume ideal mixing of 16.16.16 in an alkane solution and calculate the supersaturation for both polymorphs,[24] it is found that only the β polymorph is thermodynamically stable. Both possibilities are interesting subjects for further research.

Acknowledgment. Kees van Malssen is acknowledged for fruitful discussions on triacylglycerol crystals and carefully reading the manuscript.

References and Notes

(1) Bennema, P.; Vogels, L. J. P, de Jong, S. *J. Cryst. Growth* **1992**, *123*, 141.
(2) de Jong, S; van Soest, T. C. *Acta Crystallogr. B* **1978**, *34*, 1570.
(3) Jensen, L. H.; Mabis, A. J. *Acta Crystallogr.* **1966**, *21*, 770.
(4) Vand, V.; Bell, I. P. *Acta Crystallogr.* **1951**, *4*, 465.
(5) Larsson, K. *Arkiv Kemi* **1964**, *23*, 1.
(6) van Langevelde, A.; van Malssen, K.; Hollander, F.; Peschar, R.; Schenk, H. *Acta Crystallogr. B* **1999**, *55*, 104.
(7) de Jong, S. Thesis, University of Utrecht, 1980.
(8) Bennema, P. van der Eerden, J. P. In *Morphology of crystals*; Terra Scientific Publishing Company (TERRAPUB), 1987; p 1.
(9) Grimbergen, R. F. P.; Meekes, H.; Bennema, P.; Strom, C. S.; Vogels, L. J. P. *Acta Crystallogr. A* **1998**, *54*, 491.
(10) Meekes, H.; Bennema, P.; Grimbergen, R. F. P. *Acta Crystallogr. A* **1998**, *54*, 501.
(11) Grimbergen, R. F. P.; Bennema, P.; Meekes, H. *Acta Crystallogr. A* **1999**, *55*, 84.
(12) Vogels, L. J. P.; Marsman, H. A. M.; Verheijen, M. A. *J. Cryst. Growth* **1990**, *100*, 439.
(13) Skoda, W.; van den Tempel, M. *J. Cryst. Growth* **1967**, *1*, 207.
(14) Skoda, W.; Hoekstra, L. L.; van Soest, T. C.; Bennema, P.; van den Tempel, M. *Kolloid Z. Z. Polym.* **1967**, *219*, 149.
(15) Albon, N.; Packer, A. *Nature* **1965**, *207*, 87.
(16) Hartman, P.; Perdok, W. *Acta Crystallogr.* **1955**, *8*, 49; *Acta Crystallogr.* **1955**, *8*, 521; *Acta Crystallogr.* **1955**, *8*, 525.
(17) Dauber-Osguthorpe, P.; Roberts, V. A.; Osguthorpe, D. J.; Wolff, D.; Genest, M.; Hagler, A. T. Hagler. *Proteins: Struct. Funct. Genet.* **1988**, *4*, 31.
(18) Grimbergen, R., Meekes, H.; Boerrigter, S. X. M. C-program FACELIFT for connected net analysis, Department of Solid State Chemistry, University of Nijmegen, 1998 (hugom@sci.kun.nl).
(19) Cerius[2] User Guide, Version 3.7, PDC version, April, 1998. Molecular Simulations Inc, 9685 Scranton Road, San Diego, CA.
(20) Rijpkema, J.; Knops, H.; Bennema, P.; van der Eerden, J. *J. Cryst. Growth* **1982**, *61*, 295.
(21) van Beijeren, H.; Nolden, I. M. *Topics in current physics, structures and dynamics of surfaces II*, 43, Springer-Verlag: Berlin, 1986; pp 259−300.
(22) Hollander, F. F. A.; Plomp, M.; van Enckevort, W. J. P.; to be published
(23) Kellens, M.; Meeussen, W.; Reynaers, H. *J. Am. Oil. Chem. Soc.* **1992**, *69*, 906.
(24) Wesdorp, L. H., Thesis, Delft University, 1990.